Modification of Calcite Crystal Growth by Abalone Shell Proteins: An Atomic Force Microscope Study

Deron A. Walters,* Bettye L. Smith,* Angela M. Belcher,#§ George T. Paloczi,* Galen D. Stucky,# Daniel E. Morse,§ and Paul K. Hansma*

*Department of Physics, #Department of Chemistry, §Department of Molecular, Cellular, and Developmental Biology, University of California, Santa Barbara, California 93106, USA

ABSTRACT   A family of soluble proteins from the shell of *Haliotis rufescens* was introduced over a growing calcite crystal being scanned in situ by an atomic force microscope (AFM). Atomic step edges on the crystal surface were altered in shape and speed of growth by the proteins. Proteins attached nonuniformly to the surface, indicating different interactions with crystallographically different step edges. The observed changes were consistent with the habit modification induced by this family of proteins, as previously observed by optical microscopy. To facilitate further studies in this area, AFM techniques and certain AFM imaging artifacts are discussed in detail.

INTRODUCTION

Living creatures produce a great variety of minerals, in shapes ranging from prismatic magnetosomes in bacteria to the intricate architectures of diatoms (Lowenstam and Weiner, 1989; Simkiss and Wilbur, 1989; Webb et al., 1989). Understanding the processes that shape these minerals is of fundamental interest, but also has practical applications, from the prevention of scale formation in heat exchangers (Sikes and Wheeler, 1988), to the design of new lightweight materials (Walsh et al., 1994; Walsh and Mann, 1995), to understanding kidney and liver stone formation (Dagorn, 1993; Geider et al., 1996b; Worcester, 1994) .

One interesting process in natural systems is the control of crystal growth by soluble proteins. In various systems, proteins have been shown to control crystal phase, or the lattice structure that forms (Aizenberg et al., 1996; Belcher et al., 1996; Falini et al., 1996); crystal texture, or the size and orientation of single-crystal domains (Aizenberg et al., 1995; Berman et al., 1993); and crystal habit, or the macroscopic shape of the crystal (Berman et al., 1988; Didymus et al., 1993; Sims et al., 1995). The details of how such control takes place at a growing crystal surface are not currently known.

Binding of oyster shell proteins to a calcite surface has already been studied in air by atomic force microscopy (AFM) (Wierzbicki et al., 1994). AFM is capable of nanometer resolution on crystal surfaces (Quate, 1994; Wiesendanger, 1994) and excels at imaging a wide variety of biomolecules (Shao et al., 1996). AFM can also image under liquids, enabling processes of crystal growth to be studied in situ (Bosbach et al., 1995; Durbin et al., 1993; Hillner et al., 1992b; Malkin et al., 1995; Manne et al.,

1993). We therefore have used AFM to examine the nanometer-scale effects of shell proteins on a growing calcite surface in situ.

MATERIALS AND METHODS

Protein purification

Shells of the red abalone (*Haliotis rufescens*) were physically separated into calcitic and aragonitic portions. The calcitic portion was powdered and tested by x-ray diffraction to verify the absence of aragonite. The powder was then demineralized with acetic acid, and the resulting solution dialyzed against water to remove the acid (Belcher et al., 1996). Gel electrophoresis (Fig. 1) of the resulting protein concentrate showed it to contain a family of at least six soluble proteins, ranging in apparent molecular mass from 24 to 110 kDa. In assays by optical microscopy, this family of proteins induced a habit modification in calcite growth, yielding globular or spindle-shaped growths instead of the rhombohedra obtained in the absence of proteins (Belcher et al., 1996) .

The total protein concentration was measured by UV absorbance. Small aliquots of protein concentrate at ~1 mg/ml total proteins in water were stored at −20°C. These were thawed and diluted in calcite growth solution (see below) immediately before use.

Solution preparation

Stock solutions were prepared from reagent-grade $CaCl_2$, $NaHCO_3$, NaCl, HCl, and NaOH (Fisher, Fair Lawn, NJ; Mallinckrodt, Paris, KY) in purified water (Milli-Q; Millipore Systems, Bedford, MA). Calcite growth solutions were prepared by measuring the appropriate amounts of $CaCl_2$ and NaCl stock solutions into one container and $NaHCO_3$ solution into another. Both were diluted to slightly less than half the final volume with purified water. They were then mixed together and diluted to the final volume. With this approach, solutions more than 5× supersaturated with respect to calcite could be prepared without immediate precipitation. The data shown here were taken with 4 mM Ca^{2+} and 4 mM total carbonate; all solutions were kept at 0.5 M NaCl, to keep the total ionic strength close to that of seawater. The pH adjustments and experiments were done at room temperature (~24–25°C). Supersaturations at 25°C were estimated using the Geochemist's Workbench computer program (University of Illinois, Urbana, IL) to be 2.5× at pH 8.0, 3.1× at pH 8.1, and 3.9× at pH 8.2.
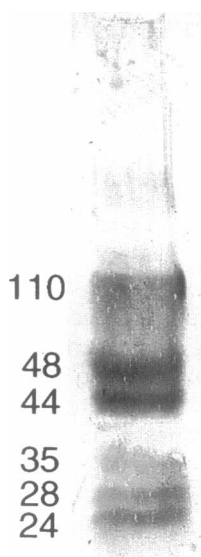
Two problems with solution stability were encountered. The solutions used in this study precipitated visible $CaCO_3$ crystals on container walls over a few weeks, accompanied by a slow downward pH drift (~0.02

FIGURE 1 The family of soluble proteins studied here. The calcitic portion of the abalone shell was demineralized in acetic acid and exhaustively dialyzed against water. Calcitic proteins were characterized by 10% Tris tricine sodium dodecyl sulfate-polyacrylamide gel electrophoresis. Proteins were blotted to polyvinylidene difluoride membrane and stained with colloidal gold. Six proteins are indicated here, with apparent molecular weights.

units/day for a pH 8.4–8.5 solution). Drift in pH was more evident for solutions at pH 8.5 and above than for a pH 8.3 solution, probably because of higher solubility at lower pH values. To avoid errors in solution concentration, solutions were made fresh biweekly or weekly and were not used after crystals were visible.

A more rapid source of pH drift was the loss of CO_2 to the atmosphere, resulting in upward pH drift. A pH 8.0 solution drifted upward by about 0.2 pH units overnight (if kept in a closed bottle) or in about 2 h if left open to the air (as in the fluid reservoir for the AFM flow-through system; see below). Drift was much faster at a pH of 7.7, but negligibly slow at a pH of 8.3. Solutions at pH > 8.0 could be stored for a few days without pH drift if kept in a sealed test tube that was completely filled (i.e., with no gas bubble into which the CO_2 could diffuse).

For best results, we therefore adjusted the pH of 50–100 ml of calcite growth solution to the desired value (generally, pH 8.0–8.1) just before imaging. The pH of the solutions was checked before and after each experiment, and before and after flowing through the AFM fluid cell. If kept for more than a few hours, the adjusted solution was stored in completely filled and sealed test tubes, and its pH was rechecked before use.

To test the effects of the proteins on calcite growth, comparisons were made between a calcite growth solution and an identical solution with proteins added ("protein-supplemented solution"). The protein-supplemented solution was usually prepared by diluting protein concentrate with a volume of calcite growth solution taken from the fluid reservoir of the already running AFM flow-through system, to minimize differences in pH and temperature between the two solutions.

Calcite sample preparation

The calcite (104) surface (cleavage face) was prepared by gluing a block of calcite (Ward's Earth Science, Rochester, NY; P&S Calcite Export, Brasilia, DF, Brazil), around 12 × 12 × 20 mm, to a 15-mm magnetic steel sample disk (Ted Pella Inc., Redding, CA) using hot-melt resin (Epon 1009F; Shell, Houston, TX). The calcite was then cleaved with a razor blade so as to leave a 12 × 12 × 1.5 mm slice stuck to the disk. The

cleaved surface was immediately wet with and incubated under a calcite growth solution to protect it from airborne contaminants. The sample was oriented in the microscope as shown in Fig. 2.

AFM imaging

AFM was performed using a commercial system (Nanoscope III Multimode; Digital Instruments, Santa Barbara, CA) in either contact mode or tapping mode. Single-crystal Si cantilevers (Ultralevers; Park Scientific Instruments, Sunnyvale, CA) were used; they generally have sharper integrated tips and lower thermal drift than silicon nitride cantilevers. The long narrow cantilever (nominal spring constant 0.16 N/m) was used for contact mode, and the short narrow cantilever (1.1 N/m) for both contact and tapping mode. Cantilevers were treated with UV light (UVP Products, San Gabriel, CA) in a closed box for at least 5 min. This has become standard laboratory procedure in our group (Thomson et al., 1996a), based on the possibility that ozone, readily detected upon opening the box, will oxidatively destroy organic contaminants on the cantilever tip. The cantilevers were hydrophilic after this treatment, suggesting that the surface groups exposed were probably Si-OH and Si-O$^-$ (Cleveland et al., 1995) .

The glass fluid cell was washed in an ethanol-water mixture and rinsed with high-performance liquid chromatography-grade ethanol (Sigma, St. Louis, MO), then thoroughly blown dry with filtered compressed air. Silicone O-rings (Pacific Rubber and Packing, San Carlos, CA) were sonicated in an ethanol-water mixture, then rinsed extensively in purified water. The O-ring was placed on the sample first, and the fluid cell was then fitted in place (Hansma et al., 1995).

Imaging parameters were chosen to compromise between maximizing the imaging speed and minimizing forces on the sample (Butt et al., 1993). Integral gain was increased until just before objects in the image developed a "shadow" due to overshoot in the feedback response (Baselt et al., 1993). Proportional gain was then increased until just before high-frequency ringing appeared in the image. The scan rate was set as high as possible without blurring of features. This gave tip speeds ranging from 80 to 220 μm/s for the data shown here.

Imaging forces in contact mode were typically on the order of 0.5–5 nN. The force was set as low as possible without letting the tip fly off the surface after crossing sample features. Maintaining the lowest possible force and quantifying the force used were made more difficult by thermal drift in the free deflection. Force variations of 0.1–0.2 nN/min were
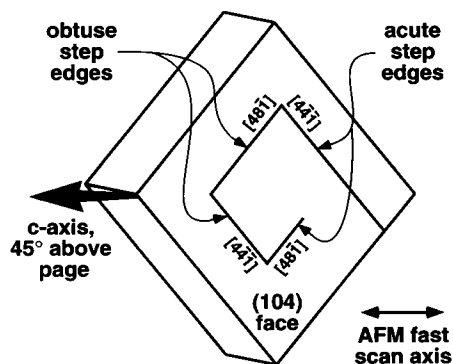
FIGURE 2 Schematic of a calcite (104) surface. Obtuse step edges grow toward a side face that forms an obtuse angle with the (104) face, as on the left (Stipp et al., 1994). Acute step edges grow toward a side face that forms an acute angle, as on the right. (Others have labeled these "positive" and "negative" step edges, respectively.) Step edges are also identified as [481] or [441] by the direction parallel to the edge. The [481] obtuse edge is a mirror image of the [441] obtuse edge; similarly, the [441] acute edge is a mirror image of the [481] acute edge. However, there is no simple relationship between an acute step edge and an obtuse step edge. This is the orientation of the samples in Figs. 3–8.

typical. In tapping mode, the driving frequency was chosen at a peak between 40 and 60 kHz in the driven response spectrum. The frequency chosen was therefore below the cantilever's resonant frequency in water. In computer simulations, this applies smaller forces to the sample than driving with a frequency above the cantilever's resonant frequency (Spatz et al., 1995). Although it is difficult to quantify the forces used in tapping mode, the setpoint was kept on the order of 10% below the free cantilever amplitude.

After the tip was brought close to the surface, fine-pitch screws in X and Y were used to translate the scan area while searching for a region that showed step edges in all four directions. One type of acceptable region featured a location where steps bud outward around the end of a crack or obstacle (as shown in Fig. 3). The best regions, however, contained a simple or compound screw dislocation, as shown in Fig. 4; these provided the clearest view of all four step edges.

The surface was always scanned first in calcite growth solution and then in protein-supplemented solution. In early experiments, a new solution was injected from one syringe while the old solution was withdrawn through a second syringe. This injection method allowed operation without an O-ring on calcite surfaces with visible macrosteps. However, during injection of the new solution, the cantilever tip was often pushed into the surface with great force by the mechanical disturbance of the imaging head, or by meniscus forces of the solution drop. In later experiments, therefore, exchange of the two solutions was handled using a continuous flow-through system (Thomson et al., 1996b), in which any of several open reservoirs could be selected to gravity-feed the fluid cell through a micrometer-controlled leak. Flow rates of 0.5 to 10 μl/s were typical. For step speed measurements, additional care was taken that the reservoirs of calcite growth solution and protein-supplemented solution were at the same level, ensuring that the flow rates through the fluid cell were the same to within 20%.

Image processing

All images shown here are in error-signal mode (Putman et al., 1992): deflection for contact mode and amplitude for tapping mode. The fast scan direction is left-to-right, so the visual effect is similar to that produced by illuminating the surface from the left. Figs. 6 and 9 were cropped to eliminate the transient at the beginning of each scan line. An overall linear fit in X (plane fit) was subtracted from Figs. 4 and 8, an overall cubic fit in X from Fig. 5, and an overall linear fit in X and Y from Fig. 6. Line-by-line cubic fits were subtracted from Fig. 9.

RESULTS AND DISCUSSION

Switching from calcite growth solution to protein-supplemented solution produced marked changes in the morphology of the calcite (104) surface (Figs. 3 and 4). Fig. 3 a shows the calcite surface in the absence of proteins. Step edges are composed of straight segments with some kinks. Corners between different step edges are sharp; this results from the highly anisotropic step edge speed as a function of direction along the surface. The acute step edges (right side) are more rounded than the obtuse step edges (left side), possibly because of a different step edge energy for these crystallographically different steps.

In Fig. 3 b the surface has been exposed to protein-supplemented solution for $\sim$350 s. The corners between step edges have become rounded, especially the corner between the obtuse step edges. This suggests that the step edge speed is now more isotropic. More rounded, isotropic step edges should produce rounded macroscopic structures, which is consistent with the habit modification produced by
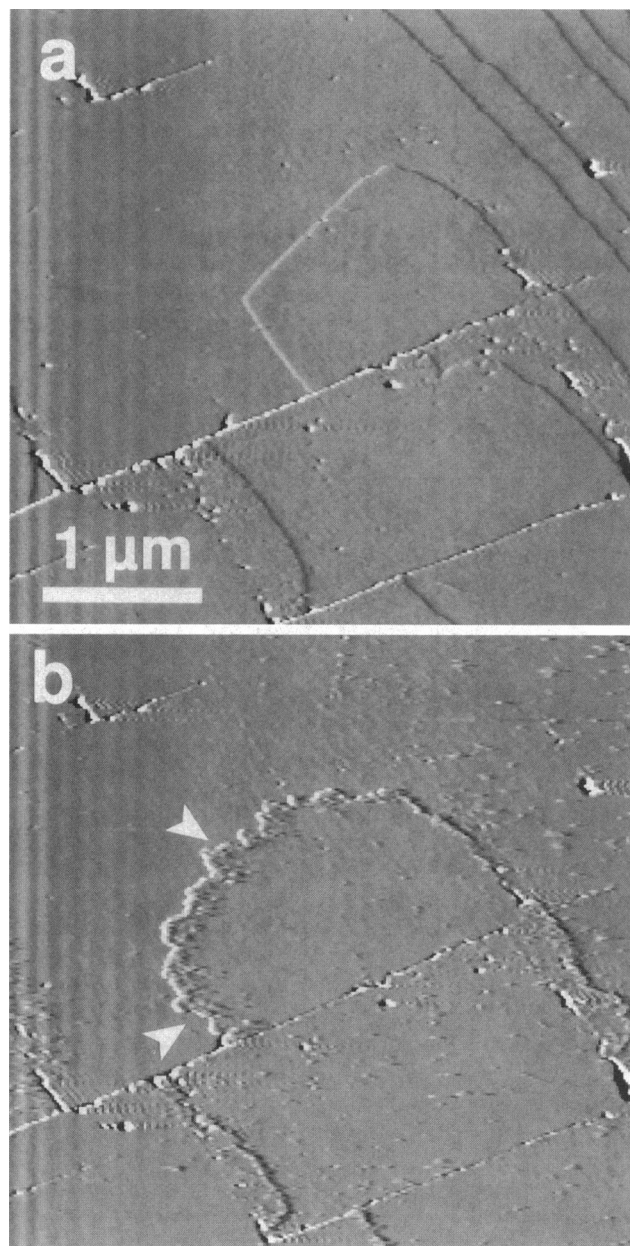

FIGURE 3 (a) A calcite (104) surface without proteins. Light grey and dark grey lines are obtuse and acute step edges, respectively. Step edges are generally straight and smooth, with sharp corners. Some kinks are visible in the acute step edges in the upper right corner. (b) With proteins. Step edges have become rounded (suggesting an isotropic step edge speed) and more convoluted. The step edge appears highlighted, as by a raised lip of proteins. Strong white-and-black features that are identical in a and b are defects in the crystal that can act as barriers to step edge motion. Conditions: pH 8.1, 2 μg/ml proteins, flow rate = 4 μl/s, 9.3 s/image, contact mode.

these proteins (Belcher et al., 1996). Step edges also appear more convoluted or kinked in the presence of proteins, resembling step edges in a defect-rich region of the crystal (Hillner et al., 1992a) or in the presence of ethanol or growth poisons (Gratz and Hillner, 1993).

Another noteworthy feature in Fig. 3 b is that the step edges appear highlighted. In the absence of proteins (Fig. 3
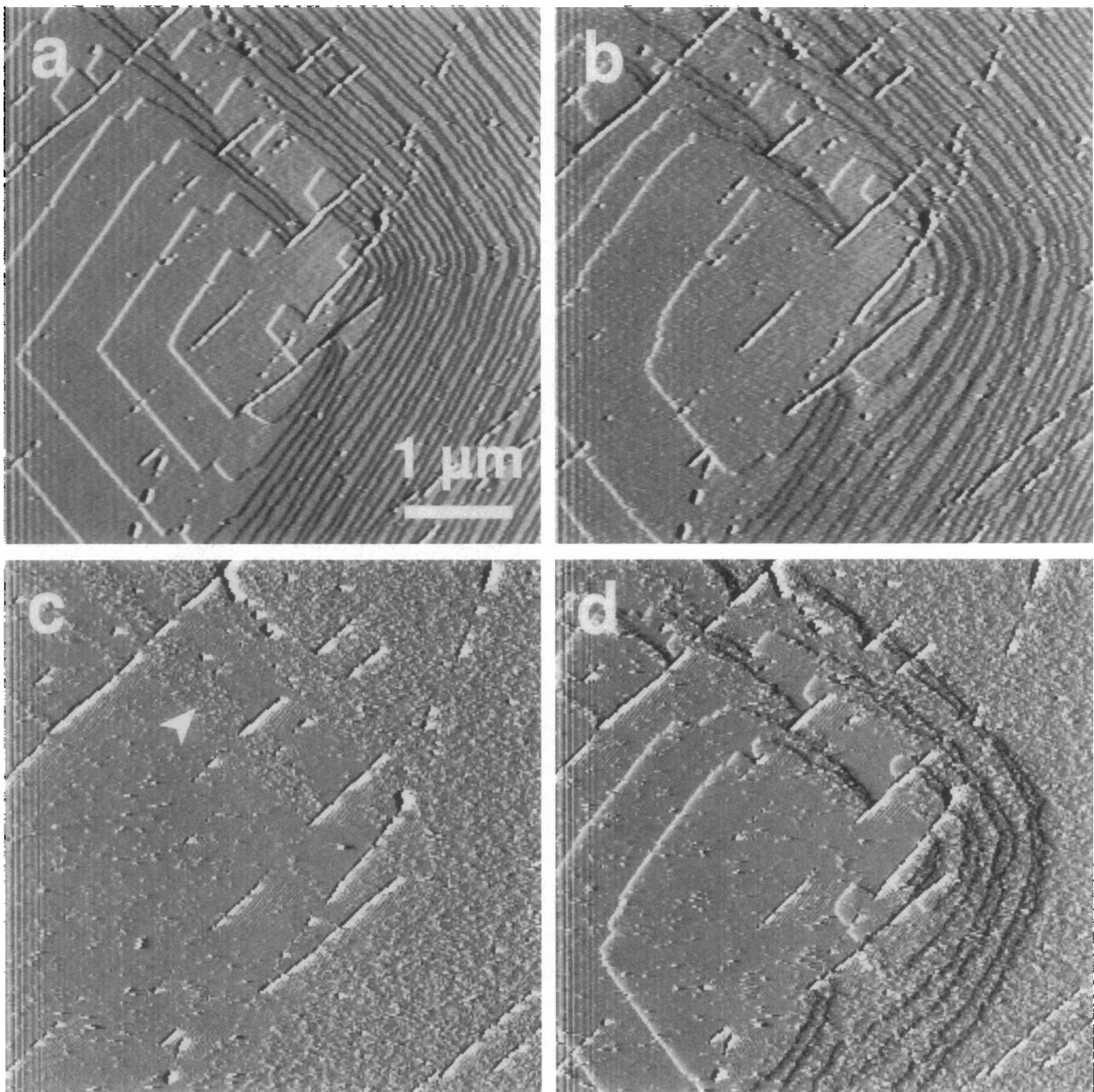
FIGURE 4   (a) A different calcite (104) surface without proteins (tapping mode). Step edges are nucleating at regular intervals from a defect near the center of the image. The corner between the acute step edges is slightly rounded, even in the absence of proteins. (b) With proteins. Step edges are rounded, but not as much as in Fig. 3 b; no highlighting is visible. (c) Contact mode image of same region. The defect has stopped nucleating step edges, and existing edges have moved outward beyond the scan area. Although all regions of this single terrace are crystallographically equivalent, there is a rough region in the right side of the image and a sharp-edged band of roughness indicated by the arrow. (d) The defect has nucleated more step edges, showing that the rough regions correspond to regions where acute step edges pass. The band is produced by acute step edges budding around the lower left end of another defect, which are met by a band of obtuse step edges budding around the upper right end. Conditions: pH 8.1–8.2, 1 μg/ml proteins, flow rate = 0.6 μl/s, 21.0 s/image.

a), each step edge appears as a single light or dark line, indicating that the edge is a simple step. With proteins present (Fig. 3 b), each edge consists of a light line followed by a dark line or vice versa. This indicates that there is a raised lip at the step edge. We attribute this to an agglomeration of proteins near the step edge. Comparing the highlighting of the [48$\bar{1}$] obtuse edge (top arrow) with the [44$\bar{1}$] obtuse edge (bottom arrow), we see an apparent symmetry about the horizontal axis (which corresponds to the ($\bar{1}$20)

glide plane). A similar apparent symmetry was observed between the highlighting of the [48$\bar{1}$] acute edge and the [44$\bar{1}$] acute edge (data not shown).

Fig. 4 a shows the surface of another sample without proteins. Upon the addition of proteins, rounding of the step edges is apparent (Fig. 4 b), albeit less pronounced than in Fig. 3. No highlighting is seen; in fact, no features can be identified as proteins on the surface. This was sometimes the case in tapping mode. In Fig. 4 c we examine the same
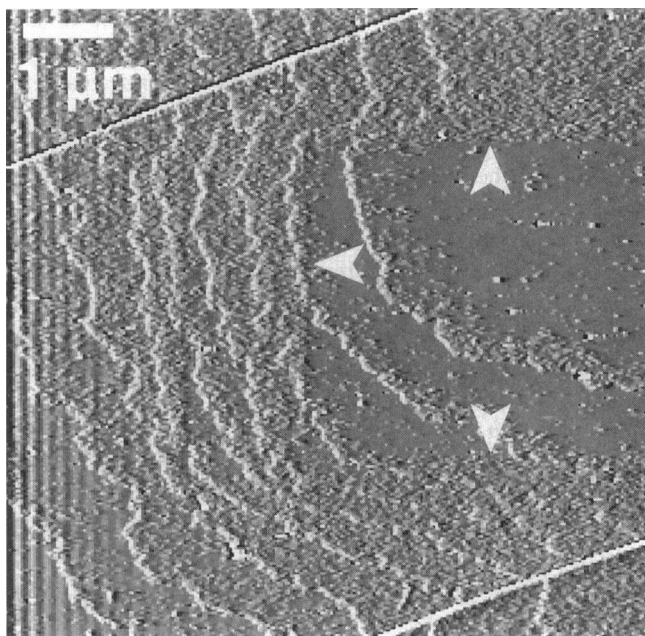
FIGURE 5   Large-area image of proteins scraped away by contact-mode
AFM. All step edges here are obtuse, growing from upper right to lower
left. The cleared region (*arrows*) was scanned for several minutes before
zooming out to collect this image. Outside the former scan area, terraces
appear densely covered with protein; within it, the terraces are clear,
leaving the edges highlighted. This suggests that proteins attach more
strongly to the step edges than to the terraces, and that the AFM tip in
contact mode scrapes away the most loosely bound. Conditions: pH 8.1, 1
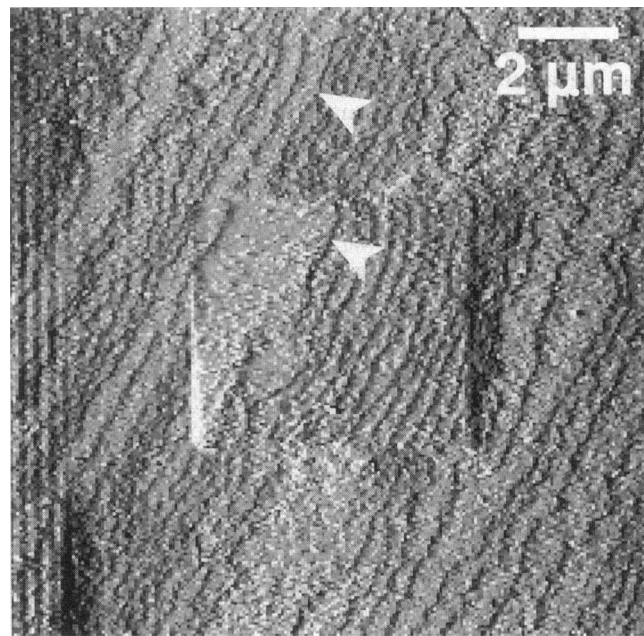μg/ml proteins, 13.1 s/image.

FIGURE 6   Acceleration of growth by contact-mode AFM. Only acute
step edges are present, growing from upper left to lower right. The square
region in the center was scanned for several minutes before zooming out to
collect this image. Because the former scan area is bounded by a white bar
on the left and a black bar on the right, it must be higher than its
surroundings. This is due to faster step edge speeds in the former scan area,
as seen by tracing the step edge marked with arrows. This step has
advanced further within the former scan area than outside it. Scan-accel-
erated growth was only seen in the presence of proteins. Conditions: pH
~7.6, 5 μg/ml proteins, flow rate = 2 μl/s, 17.3 s/image.

region in contact mode. At this time, all step edges have
moved outward beyond the scan area, such that the entire
field is a single (104) terrace. Curiously, not all regions of
the terrace are uniformly smooth, even though they are
crystallographically identical. There appear to be sharp
boundaries starting at center right and extending toward the
upper left and lower left. In the region to the left of these
boundaries, the surface is smoother than in the region to the
right, except for a diagonal band of roughness in the left
region (*arrow*). In Fig. 4 *d*, the source of steps at center right
has started up again, revealing that the rough areas are
regions of the surface that have been swept over by acute
step edges. Smooth regions have only been swept over by
obtuse step edges.

The roughness appears to consist of individual proteins
bound to the terraces. They remain in place as the crystal
continues to grow, suggesting that they are enclosed and
occluded by the crystal. This is consistent with many well-
documented examples of soluble proteins occluded in
$CaCO_3$ biominerals, such as the nacre of *H. rufescens*
(Belcher et al., 1996), the spines of the sea urchin *Paracen-
trotus lividus* (Albeck et al., 1993, 1996; Berman et al.,
1988), the prismatic layer in the shell of the mollusc *Atrina
rigida* (Albeck et al., 1993, 1996), and the spicules of the
sponge *Clathrina coriacea* (Aizenberg et al., 1994, 1996) .

One explanation for the differential roughening is that the
proteins might interact more strongly with the surface in the

vicinity of an acute step edge rather than an obtuse step
edge, binding to the surface just as the acute step edge
sweeps past. This binding could be specific, with the pro-
teins possessing a specific binding site akin to the active site
of an enzyme. Or it could be nonspecific, resulting from
electrostatic or van der Waals forces; in this case it is more
difficult to explain the clear difference in binding between
regions of acute and obtuse step edges. An alternative
explanation is that, in the absence of proteins, growth at
acute step edges might produce more defects than growth at
obtuse step edges. These supposed defects might then act as
preferential binding sites for the proteins. However, no
evidence for these defects was seen while the surface was
examined in the absence of protein.

Once again, we see in Fig. 4 an apparent symmetry about
the horizontal axis. Although the proteins distinguish an
acute step edge from an obtuse step edge, they do not appear
to distinguish a [48$\bar{1}$] obtuse edge from a [4$\bar{4}$1] obtuse edge,
or a [48$\bar{1}$] acute edge from a [4$\bar{4}$1] acute edge. This is
puzzling, because a [48$\bar{1}$] obtuse edge is, locally, the mirror
image of a [4$\bar{4}$1] obtuse edge (same for a [48$\bar{1}$] acute edge
and a [4$\bar{4}$1] acute edge). Because proteins are in general
chiral, we might expect a putative binding site to be chiral
as well. The binding of that site to a step edge and its mirror
image should then be completely different. Yet this is not
observed.

Several interpretations are possible. Either the local environment of the step edge or the binding site of the proteins may be achiral, leading to an interaction that is mirror-symmetrical. The proteins may interact only with K+ kink sites (present on both obtuse step edges) or with K− kink sites (present on both acute step edges), but not with L+ or L− kink sites nor with complete step edges (see Gratz et al., 1993, for kink site terminology). The binding may indeed be nonspecific, in which case the proteins' ability to distinguish acute from obtuse step edges needs explanation. Finally, the protein-supplemented solution contains a population of several distinct proteins (Fig. 1); one protein may interact with the [481] acute edge and a different protein with the [441] acute edge to produce the apparent symmetry we observed. Further experiments with purified individual species of protein are needed to investigate this possibility.

As can be seen from Figs. 3 and 4, the morphological changes exhibited some variability under slightly varying experimental conditions. Rounding of the step edges was the most consistent change, appearing in all experiments but one; however, the extent of rounding was not always the same. Highlighting of step edges and differential roughening in regions of acute step edges were sometimes absent. Some possible reasons for this variability include dependence on protein concentration, flow rate, or pH, beyond the precision to which we controlled them. Furthermore, different proteins within the population may have varied in their relative activities, causing different morphological changes to appear more or less strongly.

Although AFM provides a unique view of the motion and morphology of steps on the surface, it can interfere with the processes of protein-modified growth (Figs. 5 and 6). The sample in Fig. 5 was scanned in contact mode for several minutes in the presence of proteins. The scan size was then increased from 3.5 μm to 7 μm, and this image was collected. The former scan area is visible as the smooth square region marked by arrows. Outside this region, many of the terraces appear entirely covered with proteins. Within it, the step edges appear highlighted and the terraces are clear, much as in Fig. 3.

This raises the possibility that the surface is uniformly covered with proteins, and the AFM tip selectively removes the most loosely bound. This would imply that the step edges are stronger binding sites than the terraces. Alternatively, proteins could collect at the step edges in the same way that dust swept over a tabletop collects in the cracks, simply because it is geometrically protected there. We consider this unlikely because highlighted steps appeared similar in the left-to-right trace (in this case, sweeping "dust" into the step edges) and in the right-to-left trace (sweeping out of the step edges).

Another effect of AFM scanning is shown in Fig. 6. The sample was scanned in contact mode in the presence of proteins at a scan size of 5 μm and was then scanned at a larger scan size to collect this image. The former scan area is in the center of this image. As shown by the light vertical bar on its left boundary and the dark bar on its right boundary, the former scan area is raised relative to its

surroundings. Scanning with the AFM has accelerated growth in this area. This is confirmed by following the step edge indicated by the arrows: inside the former scan area, it has advanced further toward the lower right corner of the image. Other step edges are bunched together at the right boundary of the former scan area, where they have slowed down after passing out of the scan area. Although this sample was imaged with a force of 9 nN, we have observed scan-accelerated growth with an imaging force as low as ~0.8 nN; this is the lowest force we can quantify, given thermal drifts during the experiment. At our supersaturations and flow rates, no such effect was observed in the absence of proteins.

Erosion of a crystal surface in the region scanned by an AFM probe has been carefully studied (Durbin et al., 1993; Hu et al., 1995; Macpherson et al., 1996; Miyake, 1994; Thundat et al., 1993). Scan-accelerated growth has been
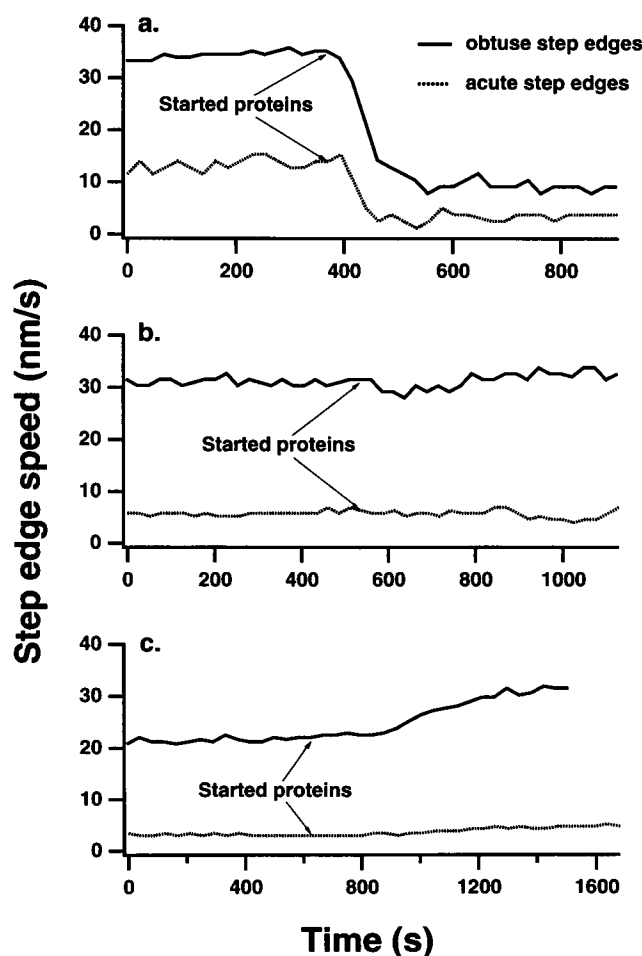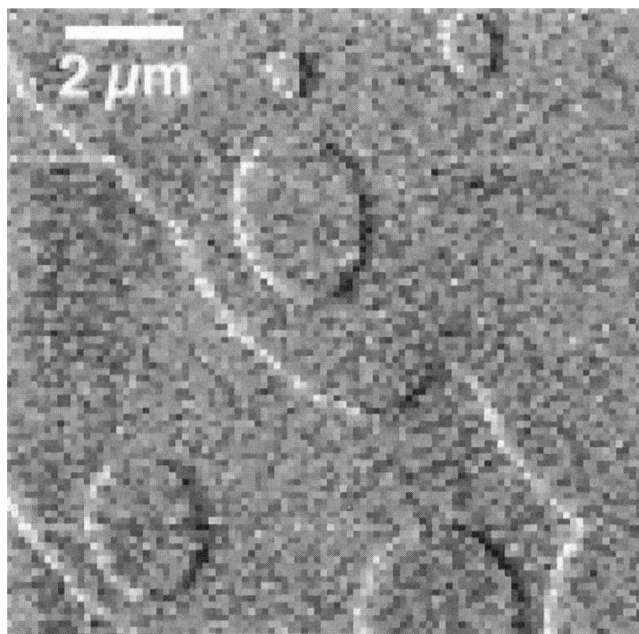

FIGURE 7 The variety of effects proteins can have on step edge speed (all in tapping mode). (a) Strong inhibition. Conditions: pH 8.0, 2 μg/ml proteins, flow rate = 5 μl/s, 11.5 s/image. (b) No effect. Conditions: pH 8.1, 1 μg/ml proteins, flow rate = 5 μl/s, 17.3 s/image. (c) Slight acceleration. Conditions: pH 8.1–8.2, 1 μg/ml proteins, flow rate = 0.6 μl/s, 21.0 s/image (same experiment as Fig. 4). Note: the time marked is when the flow of proteins was started; depending on flow rate, there is a slight delay before the proteins reach the fluid cell.
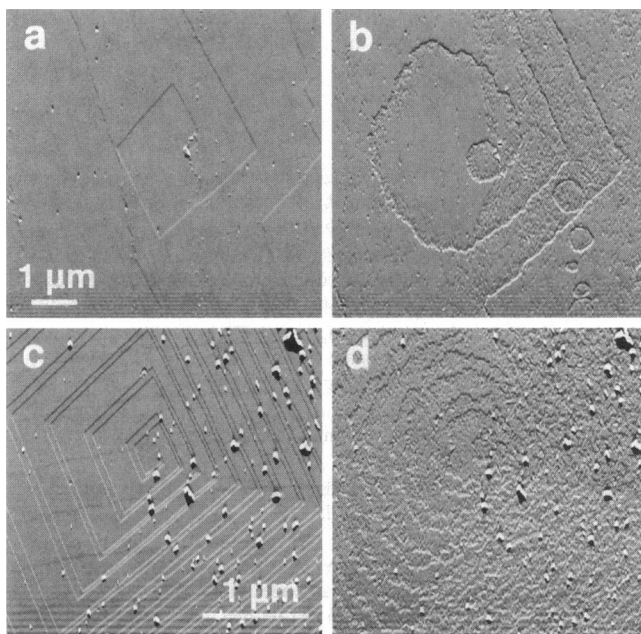
FIGURE 8 Comparison of the effects of the calcitic family of proteins, as displayed above, with the aragonitic family of proteins (extracted from a different portion of the shell). (*a*) Calcite surface without proteins. (*b*) With calcitic proteins. Note rounding and highlighting of step edges, and differential roughening of terraces in regions of acute step edges. (The vertical row of circular 2D islands (*right of center*) appeared while that vertical strip was scanned at very high force during solution exchange.) (*c*) Another calcite surface without proteins. (*d*) With aragonitic proteins at the same concentration. The step edges have become highly convoluted, and all terraces have become so rough that the step edges are barely distinguishable. Conditions: pH ~8, 5 μg/ml proteins, injection method, 26.2 s/image for *a* and *b*, 16.0 s/image for *c* and *d*, contact mode. AFM fast scan direction is bottom-to-top in this figure only, creating a visual impression of lighting from the bottom of the figure.

FIGURE 9 Two-dimensional island nucleation in the presence of 63 mM Mg^{2+}. Nucleation events occurred several seconds apart in this area of ~100 μm^2. In some experiments, island nucleation was observed at a contamination particle or a site where the AFM tip impacted on the surface, but never with this high a frequency over a large region. Conditions: pH ~8, 10 mM Ca^{2+}, 5 mM total carbonate, no proteins, no flow, 12.5 s/image. The *c* axis points out of the page toward the top of the image on this figure only.

observed before in the AFM of protein crystals (Land et al., 1995; Yip and Ward, 1996), in which case it was attributed to the AFM tip improving the diffusion of solutes from bulk solution to the crystal surface. However, a similar effect in AFM of copper electrodeposition on copper crystals (La-Graff and Gewirth, 1995) was due to removal of a protecting adlayer of oxygen atoms. Under the conditions we used in our experiments, we have not seen scan-accelerated growth after scanning in tapping mode. Because tapping mode should affect bulk diffusion in a manner comparable to that of contact mode, a mechanism highly local to the surface may be responsible.

In addition to altering the surface morphology, proteins alter the kinetics of step edge motion on the (104) calcite surface (Fig. 7). Because we did not observe the artifacts in Figs. 5 and 6 after scanning in tapping mode, step-edge speeds were only measured from tapping-mode scans. A large-area scan was analyzed after the experiment to check that step edges were not bunched together at the boundary of the former scan area. We have not yet systematically studied the kinetics as a function of protein concentration and pH; however, under varying conditions we have ob-

served three different effects on the step edge speed. Fig. 7 *a* shows slowing of both acute and obtuse step edges by a factor of 3.8. Fig. 7 *b* shows a negligible effect, and Fig. 7 *c* shows acceleration of the obtuse step edges with some possible effect on acute step edges. In Fig. 7, *a* and *b*, the pH of fluid leaving the fluid cell varied by less than 0.05 throughout the experiment. In Fig. 7 *c* the pH of fluid leaving the fluid cell was 8.22 before proteins and 8.14 after proteins were added. However, this decrease in pH would tend to make the step edge speed decrease, because calcite is more soluble at lower pH. We therefore believe that the change in pH during the experiment was not responsible for the increase in step edge speed in Fig. 7 *c*.

CONCLUSION

The resolution of the atomic force microscope has enabled us to visualize in situ the interaction between abalone shell proteins and a growing calcite (104) surface. The proteins induce rounding of the step edges on that surface, which is consistent with the macroscopic habit modification these proteins induce. Both acceleration and inhibition of step edge motion occur, depending on conditions. The proteins cause a roughening of the terraces that distinguishes between obtuse and acute step edges, but does not appear to distinguish between a step edge and its mirror image. Although this is surprising in light of the chiral nature of

Biophysical Journal

proteins, a population of several proteins was used. Further experiments with the individual proteins may reveal greater specificity.

APPENDIX

Comparison of different protein families

The aragonitic portion of the abalone shell harbors a different family of proteins from the calcitic portion discussed above (Belcher et al., 1996). The aragonitic family of proteins was extracted in similar fashion and found to contain at least three soluble proteins, ranging in apparent molecular mass from 16 to 31 kDa. When added to a calcite growth solution, they induce aragonite deposition. The resulting aragonite needles overgrow the faces of preexisting calcite crystals in the solution. This change in crystal phase caused by the aragonitic proteins is distinct from the habit modification induced by the calcitic proteins.

Just as the macroscopic effects are different, so are the microscopic effects. Fig. 8, a and b, shows the morphological changes characteristic of the calcitic proteins: rounding of step edge corners, highlighting of step edges, and differential roughening of terraces in regions of acute step edges. In contrast, Fig. 8, c and d, shows the changes caused by the aragonitic proteins at the same concentration: extensive kinking of the step edges and roughening of the entire surface, to the point that the step edges are barely distinguishable. Over a few minutes of exposure to the aragonitic proteins, the step edges were observed to grow progressively more kinked or convoluted, and their motion slowed to a stop (data not shown). Although the formation of aragonite needles was not observed, they will be sought in future studies.

A further comparison was made with bovine serum albumin (BSA) (Sigma). Albumins have been associated with crystal growth inhibitors in kidney stones (Dussol et al., 1995; Geider et al., 1994, 1996a). The addition of 2 μg/ml BSA to our growing calcite surface resulted in convoluted step edges with the c axis corner rounded. The terraces remained smooth in the presence of BSA, unlike both families of abalone shell proteins.

Effect of Mg^{2+} on calcite growth

In the absence of Mg^{2+}, simple or compound screw dislocations (as in Fig. 4) are the primary source of step edges on the (104) surface. Spontaneous nucleation of a new 2D island is extremely rare (Gratz et al., 1993), although we have seen nucleation occur at a contaminant particle on the surface or at a site where the AFM tip contacted the surface at high force (Fig. 8). In an attempt to better mimic the ionic environment of biomineralization in the abalone, we tried calcite growth solutions containing 63 mM Mg^{2+} and 10 mM Ca^{2+}. This led to frequent nucleation of 2D islands (Fig. 9). Step edges became more rounded, as can be seen from the shape of these islands. Another feature observed only in growth from Mg^{2+}-rich solutions was a ridgelike line, lengthening into the scan area from some outside source and presenting a barrier that steps could not subsequently cross (data not shown). One possible explanation for these features is the lattice strain resulting from different concentrations of Mg in the underlying geological calcite and the overgrown layer. In practice, the island nucleation and ridgelike lines obstructed our efforts to see protein-induced effects on crystal growth, so we restricted our study to solutions with no Mg. Similar difficulties might be encountered when filtered natural seawater or standard artificial seawater recipes are used.

REFERENCES

Aizenberg, J., S. Albeck, S. Weiner, and L. Addadi. 1994. Crystal-protein interactions studied by overgrowth of calcite on biogenic skeletal elements. *J. Crystal Growth.* 142:156–164.

Aizenberg, J., J. Hanson, T. F. Koetzle, L. Leiserowitz, S. Weiner, and L. Addadi. 1995. Biologically induced reduction in symmetry: a study of crystal texture of calcitic sponge spicules. *Chem. Eur. J.* 1:414–422.

Aizenberg, J., G. Lambert, L. Addadi, and S. Weiner. 1996. Stabilization of amorphous calcium carbonate by specialized macromolecules in biological and synthetic precipitates. *Adv. Mater.* 8:222–226.

Albeck, S., J. Aizenberg, L. Addadi, and S. Weiner. 1993. Interactions of various skeletal intracrystalline components with calcite crystals. *J. Am. Chem. Soc.* 115:11691–11697.

Albeck, S., S. Weiner, and L. Addadi. 1996. Polysaccharides of intracrystalline glycoproteins modulate calcite crystal growth in vitro. *Chem. Eur. J.* 2:278–284.

Baselt, D. R., S. M. Clark, M. G. Youngquist, C. F. Spence, and J. D. Baldeschwieler. 1993. Digital signal processor control of scanned probe microscopes. *Rev. Sci. Instrum.* 64:1874–1882.

Belcher, A. M., X. H. Wu, R. J. Christensen, P. K. Hansma, G. D. Stucky, and D. E. Morse. 1996. Control of crystal phase switching and orientation by soluble mollusc-shell proteins. *Nature.* 381:56–58.

Berman, A., L. Addadi, and S. Weiner. 1988. Interactions of sea-urchin skeleton macromolecules with growing calcite crystals—a study of intracrystalline proteins. *Nature.* 331:546–548.

Berman, A., J. Hanson, L. Leiserowitz, T. F. Koetzle, S. Weiner, and L. Addadi. 1993. Biological control of crystal texture: a widespread strategy for adapting crystal properties to function. *Science.* 259:776–779.

Bosbach, D., G. Jordan, and W. Rammensee. 1995. Crystal growth and dissolution kinetics of gypsum and fluorite: an in situ scanning force microscope study. *Eur. J. Mineral.* 7:267–276.

Butt, H.-J., P. Siedle, K. Seifert, K. Fendler, T. Seeger, E. Bamberg, A. L. Weisenhorn, K. Goldie, and A. Engel. 1993. Scan speed limit in atomic force microscopy. *J. Microsc.* 169:75–84.

Cleveland, J. P., T. E. Schaffer, and P. K. Hansma. 1995. Probing oscillatory hydration potentials using thermal-mechanical noise in an atomic-force microscope. *Phys. Rev. B.* 52:R8692–R8695.

Dagorn, J. C. 1993. Lithostathine. *In* The Pancreas: Biology, Pathobiology, and Disease. Raven Press, New York. 253–263.

Didymus, J. M., P. Oliver, S. Mann, A. L. DeVries, P. V. Hauschka, and P. Westbroek. 1993. Influence of low-molecular-weight and macromolecular organic additives on the morphology of calcium carbonate. *J. Chem. Soc. Faraday Trans.* 89:2891–2900.

Durbin, S. D., W. E. Carlson, and M. T. Saros. 1993. In situ studies of protein crystal growth by atomic force microscopy. *J. Phys. D.* 26:B128–B132.

Dussol, B., S. Geider, A. Lilova, F. Leonetti, P. Dupuy, M. Daudon, Y. Berland, J. C. Dagorn, and J. M. Verdier. 1995. Analysis of the soluble organic matrix of five morphologically different kidney stones: evidence for a specific role of albumin in the constitution of the stone protein matrix. *Urol. Res.* 23:45–51.

Falini, G., S. Albeck, S. Weiner, and L. Addadi. 1996. Control of aragonite or calcite polymorphism by mollusk shell macromolecules. *Science.* 271:67–69.

Geider, S., B. Dussol, P. Dupuy, A. Lilova, Y. Berland, J. C. Dagorn, and J. M. Verdier. 1994. Evidence that albumin (A) can induce the nucleation of calcium oxalate monohydrate (COM) crystals. *Nephrol. Dial. Transplant.* 9:908.

Geider, S., B. Dussol, C. Hennequin, S. Veesler, S. Nitsche, R. Boistelle, M. Daudon, Y. Berland, J. C. Dagorn, and J. M. Verdier. 1996a. Nucleation of calcium oxalate crystals by albumin: involvement in the prevention of stone formation. *Nephrol. Dial. Transplant.* 11:A44.

Geider, S., B. Dussol, S. Nitsche, S. Veesler, P. Berthezene, P. Dupuy, J. P. Astier, R. Boistelle, Y. Berland, J. C. Dagorn, and J. M. Verdier. 1996b. Calcium carbonate crystals promote calcium oxalate crystalliza-

tion by heterogeneous or epitaxial nucleation: possible involvement in the control of urinary lithogenesis. *Calcif. Tissue Int.* 59:33-37.

Gratz, A. J., and P. E. Hillner. 1993. Poisoning of calcite growth viewed in the atomic force microscope (AFM). *J. Crystal Growth.* 129:789-793.

Gratz, A. J., P. E. Hillner, and P. K. Hansma. 1993. Step dynamics and spiral growth on calcite. *Geochim. Cosmochim. Acta.* 57:491-495.

Hansma, H. G., D. E. Laney, M. Bezanilla, R. L. Sinsheimer, and P. K. Hansma. 1995. Applications for atomic force microscopy of DNA. *Biophys. J.* 68:1672-1677.

Hillner, P. E., A. J. Gratz, S. Manne, and P. K. Hansma. 1992a. Atomic-scale imaging of calcite growth and dissolution in real time. *Geology.* 20:359-362.

Hillner, P. E., S. Manne, A. J. Gratz, and P. K. Hansma. 1992b. AFM images of dissolution and growth on a calcite crystal. *Ultramicroscopy.* 42-44, pt. B:1387-1393.

Hu, J., X.-D. Xiao, D. F. Ogletree, and M. Salmeron. 1995. Atomic scale friction and wear of mica. *Surfactant Sci.* 327:358-370.

LaGraff, J. R., and A. A. Gewirth. 1995. Nanometer-scale mechanism for the constructive modification of Cu single crystals and alkanethiol passivated Au(111) with an atomic force microscope. *J. Phys. Chem.* 99:10009-10018.

Land, T. A., A. J. Malkin, Y. G. Kuznetsov, A. McPherson, and J. J. De Yoreo. 1995. Mechanisms of protein crystal growth: an atomic force microscopy study of canavalin crystallization. *Phys. Rev. Lett.* 75:2774-2777.

Lowenstam, H. A., and S. Weiner. 1989. On Biomineralization. Oxford University Press, New York.

Macpherson, J. V., P. R. Unwin, A. C. Hillier, and A. J. Bard. 1996. In-situ imaging of ionic crystal dissolution using an integrated electrochemical/AFM probe. *J. Am. Chem. Soc.* 118:6445-6452.

Malkin, A. J., Y. G. Kuznetsov, T. A. Land, J. J. De Yoreo, and A. McPherson. 1995. Mechanisms of growth for protein and virus crystals. *Nature Struct. Biol.* 2:956-959.

Manne, S., J. P. Cleveland, G. D. Stucky, and P. K. Hansma. 1993. Lattice resolution and solution kinetics on surfaces of amino acid crystals: an atomic force microscope study. *J. Crystal Growth.* 130:333-340.

Miyake, S. 1994. Atomic-scale wear properties of muscovite mica evaluated by scanning probe microscopy. *Appl. Phys. Lett.* 65:980-982.

Putman, C. A. J., K. O. van der Werf, B. G. de Grooth, N. F. van Hulst, J. Greve, and P. K. Hansma. 1992. New imaging mode in atomic force microscopy based on the error signal. *SPIE Proc.* 1639:198-204.

Quate, C. F. 1994. The AFM as a tool for surface imaging. *Surfactant Sci.* 299-300:980-995.

Shao, Z., J. Mou, D. M. Czajkowsky, J. Yang, and J.-Y. Yuan. 1996. Biological atomic force microscopy: what is achieved and what is needed. *Adv. Phys.* 45:1-86.

Sikes, C. S., and A. P. Wheeler. 1988. Regulators of biomineralization. *Chemtech.* 18:620-626.

Simkiss, K., and K. M. Wilbur. 1989. Biomineralization: Cell Biology and Mineral Deposition. Academic Press, San Diego.

Sims, S. D., J. M. Didymus, and S. Mann. 1995. Habit modification in synthetic crystals of aragonite and vaterite. *J. Chem. Soc. Chem. Commun.* 1031-1032.

Spatz, J. P., S. Sheiko, M. Moller, R. G. Winkler, P. Reineker, and O. Marti. 1995. Forces affecting the substrate in resonant tapping force microscopy. *Nanotechnology.* 6:40-44.

Stipp, S. L. S., C. M. Eggleston, and B. S. Nielsen. 1994. Calcite surface structure observed at microtopographic and molecular scales with atomic force microscopy (AFM). *Geochim. Cosmochim. Acta.* 58:3023-3033.

Thomson, N. H., M. Fritz, M. Radmacher, J. P. Cleveland, C. F. Schmidt, and P. K. Hansma. 1996a. Protein tracking and detection of protein motion using atomic force microscopy. *Biophys. J.* 70:2421-2431.

Thomson, N. H., S. Kasas, B. Smith, H. G. Hansma, and P. K. Hansma. 1996b. Reversible binding of DNA to mica for AFM imaging. *Langmuir.* 12:5905-5908.

Thundat, T., B. C. Sales, B. C. Chakoumakos, L. A. Boatner, D. P. Allison, and R. J. Warmack. 1993. Atomic layer-by-layer surface removal by force microscopy. *Surfactant Sci. Lett.* 293:L863-L869.

Walsh, D., J. D. Hopwood, and S. Mann. 1994. Crystal tectonics—construction of reticulated calcium phosphate frameworks in bicontinuous reverse microemulsions. *Science.* 264:1576-1578.

Walsh, D., and S. Mann. 1995. Fabrication of hollow porous shells of calcium carbonate from self-organizing media. *Nature.* 377:320-323.

Webb, J., R. J. P. Williams, and S. Mann. 1989. Biomineralization: Chemical and Biochemical Perspectives. Vch, Weinheim, Germany.

Wierzbicki, A., C. S. Sikes, J. D. Madura, and B. Drake. 1994. Atomic force microscopy and molecular modeling of protein and peptide binding to calcite. *Calcif. Tissue Int.* 54:133-141.

Wiesendanger, R. 1994. Scanning Probe Microscopy and Spectroscopy: Methods and Applications. Cambridge University Press, Cambridge.

Worcester, E. M. 1994. Urinary calcium oxalate crystal growth inhibitors. *J. Am. Soc. Nephrol.* 5:S46-S53.

Yip, C. M., and M. D. Ward. 1996. Atomic force microscopy of insulin single crystals—direct visualization of molecules and crystal growth. *Biophys. J.* 71:1071-1078.